Ultrasound in Med. & Biol., Vol. 26, No. 1, pp. 143–152, 2000

0301-5629/00/$–see front matter

PII S0301-5629(99)00113-1

● *Original Contribution*

EFFECTS OF PHASE ABERRATION ON HIGH FRAME RATE IMAGING

JIAN-YU LU and SHIPING HE
Ultrasound Laboratory, Department of Bioengineering, The University ofToledo, Toledo, OH 43606 USA

(*Received* 25 *January* 1999; *in final form* 23 *July* 1999)

Abstract—A high frame-rate (HFR) imaging method (about 3750 frames/s for imaging of biological soft tissues at a depth of 200 mm) has been developed recently with limited diffraction beams. This method uses the fast Fourier transform (FFT) and inverse fast Fourier transform (IFFT) to construct images, and can be implemented with simple and inexpensive hardware, compared to the conventional delay-and–sum method where a digital beam former is usually used. In this paper, phase aberration effects are studied for both the high frame rate and the conventional methods by adding random phase shifts to echo signals obtained from an experiment. In the study, two broadband linear arrays were used to construct images of an ATS 539 tissue-equivalent phantom that has a frequency-dependent attenuation of about 0.5 dB/MHz/cm. The first array has 48 elements, a central frequency of 2.25 MHz, an aperture of 18.288 mm, and a width of 12.192 mm in elevation. The second has 64 elements, a central frequency of 2.5 MHz, and a dimension of 38.4 mm × 10 mm. The-6dB pulse-echo bandwidth of both arrays is about 40% of their center frequencies. Radiofrequency (RF) signals were digitized at 20 mega samples/s at a 12-bit resolution to construct images. Results show that phase aberration has about the same effect on both methods in terms of image resolution and contrast, although the high frame-rate method can be implemented with a simpler system. © 2000 World Federation for Ultrasound in Medicine & Biology.

Key Words: **High frame-rate imaging, Phase aberration, Limited diffraction beam, X waves, Fourier construction, Ultrasonic imaging, Medical imaging.**

INTRODUCTION

Limited diffraction beams were first recognized by Stratton (1941) when he derived a Bessel beam solution to the isotropic-homogeneous wave equation. In 1991, other limited diffraction beams were discovered (Lu and Greenleaf 1991). Because these beams have an X-like shape in a plane along the axis of the waves and contain multiple frequencies, they have been termed X waves (Lu and Greenleaf 1992a, 1992b; Song et al. 1993; Lu et al. 1994). Theoretically, such beams can propagate to an infinite distance without changing their shapes if they are produced with an infinite aperture and energy. In practice, with a finite aperture and energy, they have a large depth of field (*i.e.*, they can propagate to a large distance without significant distortions. Because of this advantage, these beams could have applications in medical imaging (Lu and Greenleaf 1990a), tissue property identification (Lu and Greenleaf 1990b), blood flow velocity vector measurement (Lu et al. 1995; Lu 1996), nondestructive evaluation (NDE) of materials (Lu and Greenleaf 1993), communications (Lu and Shiping 1999), and other areas, such as optics (Durnin 1987; Durnin et al. 1987) and electromagnetics (Brittingham 1983; Donnelly et al. 1994; Ziolkowski 1985, Ziolkowski et al. 1989; Ojeda-Castaneda and Noyola-lglesias 1990).

Based on the extensive study of limited diffraction beams, a high frame-rate (HFR) two-dimensional (2-D) and three-dimensional (3-D) imaging method has recently been developed (Lu 1997a, 1997b, 1997c, 1997d, 1998a, 1998b). In this method, a broadband plane wave pulse is transmitted from a 1-D or 2-D array transducer to uniformly illuminate the target. Echoes returned from the targets are received with the same transducer, but weighted to produce limited diffraction responses (Lu 1997a). The weighted echoes are used to calculate the spatial Fourier transform (Bracewell 1965) of the targets. Reflectivity of 2-D or 3-D objects is constructed with a 2-D or 3-D inverse spatial Fourier transform, respectively. The HFR imaging method has a number of advantages. First, it can achieve amaximum frame rate of about 3750 frames/s for imaging of biological soft tissues at a depth of 200 mm because only one transmission is required to construct either a 2-D or 3-D image.

Address correspondence to: Jian-yu Lu, Ph.D., Professor and Director Ultrasound Laboratory, Department of Bioengineering, The University of Toledo, 2801 West Bancroft Street, Toledo, OH 43606–3390 USA. E-mail: jilu@eng.utoledo.edu

Second, imaging systems based on this method will be greatly simplified because fast Fourier transform (FFT) and inverse fast Fourier transform (IFFT) can be used. For example, the number of computations for conventional systems that are based on the delay-and–sum (dynamic focusing) algorithm (Shen et al. 1995; Wells 1977) and a digital beam former is proportional to N^5 for 3-D imaging in addition to the delay and interpolation operations, where N is roughly the number of points in one dimension of a constructed radiofrequency (RF) image and can be a few thousands in some dimension. In contrast, the number of computations required for the high frame-rate method is proportional to $N^3 \log_2 N$, which is similar to the MRI imaging (Bailes and Bryant 1984; Bronskill and Sprawls 1993). In typical medical applications, the ratio between N^5 and $N^3 \log_2 N$ is a few thousands. Third, because the entire aperture of an array is used in transmission and the transmit plane wave does not diverge within the depth of interest for most medical transducers, the signal-to–noise ratio (SNR) is high (Lu 1998b) as compared to other 3-D high frame-rate methods (Shattuck et al. 1984). Fourth, the method can easily be extended to achieve both transmit and receive dynamic focusing without montage and to construct images in a large field of view at a high resolution and contrast (Lu 1997b). Fifth, because of the potentially high frame rate, RF echo signals can be used to construct 2-D or 3-D flow vector images with speckle tracking without decorrelation (Trahey et al. 1988a; Bohs and Trahey 1991; Ramamurthy and Trahey 1991; Bohs et al. 1993, 1995). Last, the potentially high frame rate can be used to perform spatial and frequency compounding (nonlinear or incoherent processing) to smooth speckle and enhance image contrast (Trahey et al. 1986; Silverstein and O'Donnell 1987). Electronic noise can be reduced by averaging multiple volumes of images coherently.

Although the HFR imaging method has many advantages, like the conventional imaging systems, it is affected by the phase aberration of biological soft tissues. Phase aberration is caused by sound speed variations in inhomogeneous media such as biological soft tissues, causing errors in calculating propagation delay, phase, amplitude, and waveform, across the surface of the transducer array (Foster and Hunt 1979; Flax and O'Donnell 1988; O'Donnell and Flax 1988; Trahey et al. 1991; Zhao and Trahey 1991; Zhao et al. 1992; Nock and Trahey 1992; Trahey and Nock 1992; Krishnan et al. 1995,1996; Li and O'Donnell 1995). Because all beam formers are designed by assuming a constant speed of sound, phase aberration may degrade image quality (Foster et al. 1989). The phase aberration is more serious when a larger array or a higher operating frequency is employed to increase resolution. In this paper, effects of phase aberration on the HFR imaging method are studied experimentally and are compared to those of the delay-and–sum method. In the experiment, two broadband linear arrays were used to obtain images of an ATS 539 tissue-equivalent phantom with a frequency-dependent attenuation of 0.5dB/MHz/cm. The first array had 48 elements, a 2.25-MHz center frequency, and was 18.288 mm $\times$ 12.192 mm in dimension, with an element spacing (distance between the centers of two adjacent elements) of about 0.381mm. The second array had 64 elements, a larger aperture (38.4 mm $\times$ 10 mm), a higher center frequency (2.5 MHz), and also a larger element spacing (0.6 mm). To study the phase aberration effects, random time (phase) shifts were applied to echo signals received by the array elements (notice that the phase aberration on transmit beam is ignored here). Results show that the quality of constructed images is degraded as the magnitude of the random phase shift increases. However, the effects of phase aberration are about the same on both the HFR and the delay-and–sum methods in terms of resolution, side lobes, and image contrast, although imaging systems based on the HFR method can be greatly simplified.

THEORY OF 2-D AND 3-D HFR IMAGING

Here, the theory of HFR imaging is briefly reviewed. Details can be found in Lu (1997a, 1997b, 1997c, 1997d, 1998a).

Let us assume that a 3-D object, with $f(\vec{r})$ (reflection coefficient), is composed of randomly positioned point scatterers embedded in a uniform background supporting a constant speed of sound. The received signal from the entire object, $f(\vec{r})$, is given by the following convolution (Lu 1997a):

$$R_{k_x,k_y,k_z'}(t) = \int_V f(\vec{r})[P(z - ct) * \Phi_{\text{Array}}(\vec{r}, t)]d\vec{r}$$

$$= \frac{1}{2\pi}\int_{-\infty}^{\infty} \frac{A(k)T(k)H(k)}{c} \times F(k_x, k_y, k_z')e^{-i\omega t}dk, \quad (1)$$

where * represents the convolution with respect to time,

$$P(z - ct) = \frac{1}{2\pi}\int_{-\infty}^{\infty} \frac{A(k)e^{ikz}}{c} e^{-i\omega t}d\omega \quad (2)$$

is a broadband plane wave with its transmit transfer function of $A(k)$, (see eqn. (4) of Lu and Greenleaf 1992a), c is the speed of sound, z is the distance to transducer surface, $k = \omega/c$ is the wave number, ω is the

angular frequency, t is the time, V is the volume of scatterers illuminated with the plane wave,

$$\Phi_{\text{Array}}(\vec{r},\, t) = \frac{1}{2\pi}\int_{-\infty}^{\infty} T(k)\, H(k) e^{ik_x x + ik_y y + ik_z z} e^{-i\omega t} dk \quad (3)$$

is a limited diffraction array beam with a transfer function of *T(k)* (Lu 1997c, 1997d),

$$H\left(\frac{\omega}{c}\right) = \begin{cases} 1 & , \quad \omega \geq 0 \\ 0 & , \quad \omega < 0 \end{cases} \quad (4)$$

is the Heaviside step function (Bracewell, 1965a), k_x and k_y are weighting parameters of the array beam,

$$k_z = \sqrt{k^2 - k_x^2 - k_y^2},\; k_z' = k + k_z, \quad (5)$$

and $F(k_x\,, k_y\,, k'_z\,)$ is the Fourier transform of the object function. Here, we assume that the imaging system is linear (approximately true in medical ultrasonic imaging). The limited diffraction array beam in eqn (3) represents the received time signal from a point source located at $\vec{r} = (x, y, z)$. Notice that k_x and k_y in eqn (3) can be chosen to obtain different receive signals so that the Fourier transform of the object function, $F(k_x\,, k_y\,, k'_z\,)$, is known on rectangular grids of the spatial Fourier domain. Such choice of the parameters will allow subsequent FFT and IFFT algorithms to be applied directly.

From eqn (1), one obtains a band-limited version of the spatial Fourier transform of the object function,

$$F_{BL}(k_x,\, k_y,\, k_z') = c^2 H(k) \tilde{R}_{k_x,k_y,k_z'}(\omega), \quad (6)$$

where

$$\tilde{R}_{k_x,k_y,k_z'}(\omega) \quad (7)$$

is the temporal Fourier transform of

$$R_{k_x,k_y,k_z'}(t). \quad (8)$$

H(k) indicates that only positive values of k are used and, thus, it can be applied to either side of the equation (for the convenience of presentation, it is used with

$$\tilde{R}_{k_x,k_y,k_z'}(\omega), \quad (9)$$

and

$$F_{BL}(k_x,\, k_y,\, k_z') = A(k) T(k)\, F(k_x,\, k_y,\, k_z'), \quad (10)$$

where the subscript *BL* means "band-limited." In practical systems, *A(k)T(k)* is always band-limited and, thus, it can be assumed, for example, to be proportional to the Blackman window function (Oppenheim 1975):

$$W(k) = \begin{cases} 0.42 - 0.5\cos\dfrac{\pi k}{k_0} + 0.08\cos\dfrac{2\pi k}{k_0}, & 0 \leq k \leq 2k_0 \\ 0, & \text{otherwise} \end{cases}, \quad (11)$$

where $k_0 = 2\pi f_0/c$ and f_0 is the center frequency. The −6-dB bandwidth of *W(k)* is about 81% of its center frequency, which is typical for modern medical US transducers. If the object function, $f(\vec{r})$, is real, which is the case in most applications, we have

$$F(-k_x,\, -k_y,\, -k_z') = F^*(k_x,\, k_y,\, k_z'), \quad (12)$$

where the superscript * means complex conjugation. In this case, the spatial Fourier transform of the object function in the lower Fourier space ($k' < 0$) is also known. Taking an inverse spatial Fourier transform of eqn (6), one can approximately construct 3-D images (Lu 1997a, 1998a). A close-form formula (Lu 1997a, 1998a) can also be used to construct images

$$f(\vec{r}) \approx \frac{c^2}{(2\pi)^3}\int_0^{\infty} k^2 dk \int_{-\pi}^{\pi} d\theta \int_0^{\pi/2} \sin\zeta(1+\cos\zeta) \cdot d\zeta \tilde{R}'_{k,\zeta,\theta}(\omega) e^{-ikr\sin\zeta\cos(\phi-\theta) - ik(1+\cos\zeta)z}, \quad (13)$$

where r is radial distance, ζ ($0 \leq \zeta < \pi/2$) is the Axicon angle of X waves (Burckhardt1973a, 1973b; Lu and Greenleaf 1992a, 1992b), θ ($-\pi \leq \theta < \pi$) is an initial angle of X waves around the wave axis (Lu 1997a),

$$\tilde{R}'_{k,\zeta,\theta}(\omega) = \tilde{R}_{k_x,k_y,k_z'}(\omega), \quad (14)$$

and the approximation in eqn (13) is due to the fact that any physical system is band-limited and only part of the Fourier space is known from backscattered data because the aperture of a transducer is finite.

Similarly, if the object function is 2-D (*i.e.*, $f(\vec{r}) = f^{(2)}(x,z)$, where the superscript (2) means 2-D B-mode, one obtains the relationship between the received signals and the Fourier transform of the object function

$$R^{(2)}_{k_x,k_z'}(t) = \frac{1}{2\pi}\int_{-\infty}^{\infty} \frac{A(k)T(k)H(k)}{c} F^{(2)}(k_x,\, k_z') e^{-i\omega t} dk, \quad (15)$$

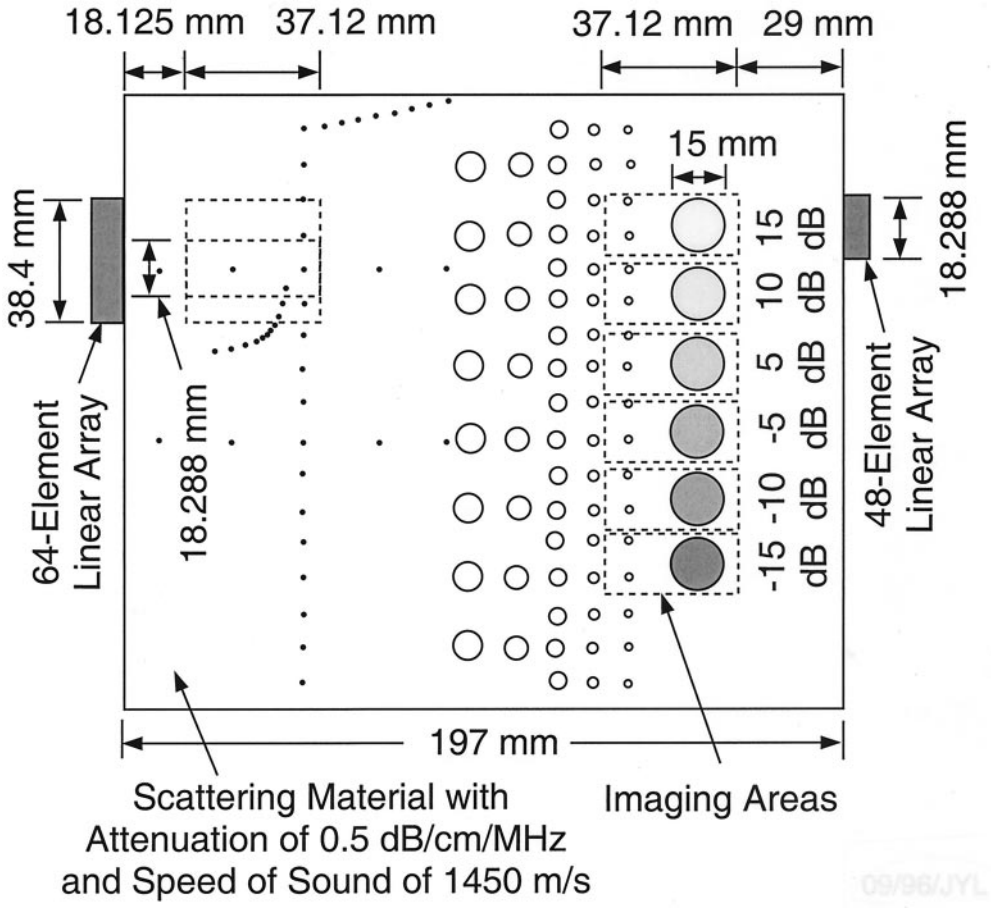

Fig. 1. A cross-section of an ATS539 multipurpose rubber-based tissue-equivalent phantom for 2-D B-mode imaging. It is composed of line scatterers, grey-scale cylindrical objects, and anechoic cylindrical objects. All the objects are embedded in a background of random scatterers. The contrasts of the grey-scale objects are ranged from −15 dB to +15 dB relative to the background. Dashed rectangular boxes are areas where 2-D B-mode images are to be constructed (reproduced from Fig. 2 of Lu 1998a, with permission).

where $F^{(2)}(k_x, k'_z)$ is a spatial Fourier transform of $f^{(2)}(x,z)$.

From eqn (15), one obtains, similar to eqns (6) and (10):

$$F^{(2)}_{BL}(k_x, k'_z) = A(k)T(k)F^{(2)}(k_x, k'_z) = c^2 H(k)\tilde{R}^{(2)}_{k_x,k'_z}(\omega), \tag{16}$$

where

$$\tilde{R}^{(2)}_{k_x,k'_z}(\omega) \tag{17}$$

is the temporal Fourier transform of

$$R^{(2)}_{k_x,k'_z}(t). \tag{18}$$

2-D B-mode images can be constructed approximately with an inverse 2-D spatial Fourier transform of eqn (16) or with the close-form formula (Lu 1997a)

$$f^{(2)}(x, z) \approx \frac{c^2}{(2\pi)^2}\int_0^{\infty} kdk \int_0^{\pi/2} (1 + \cos\zeta) \cdot d\zeta \tilde{R}^{(2)\prime}_{k,\zeta}(\omega) e^{-ikx\sin\zeta - ik(1+\cos\zeta)z} \tag{19}$$

where

$$\tilde{R}^{(2)\prime}_{k,\zeta}(\omega) = \tilde{R}^{(2)}_{k_x,k_z}(\omega) \tag{20}$$

and the approximation $\approx$ is due to the finite bandwidth and finite aperture size of the transducer.

From the theoretical analysis, image constructions

with the HFR method can be summarized in the following steps:

1. Transmit a broadband pulse plane wave (eqn (2)) to illuminate scatterers in a region of interest (the illumination is collimated and is similar to the beam of a flashlight);
2. Echoes from the scatterers are received with the same array transducer that is used in transmit;
3. Multiple weighting functions are applied simultaneously with different weighting parameters (k_x and k_y) to form limited diffraction array beam responses given by eqn (3);
4. Received signals after the weightings (eqn (1)) are Fourier transformed with FFT in terms of time and then interpolated to get spatial Fourier transform on rectangular grids along the k'_z dimension. 2-D and 3-D images are constructed with spatial IFFT transformations of eqns (6) and (16), respectively.

In these steps, the complicated conventional digital beamforming is not needed for the HFR method because electronic delays of received signals are not necessary.

EXPERIMENT AND RESULTS

To study the effects of phase aberration on the HFR imaging method developed in the last section, an experiment was carried out. In the experiment, a commercial tissue-equivalent phantom (ATS 539, ATS Laboratories, Inc., Bridgeport, CT) was used (Fig. 1). This phantom consists of cylindrical objects of different scattering coefficients relative to the background. The contrasts of these objects are −15 dB, −10 dB, −5 dB, 5 dB, 10 dB and 15 dB, respectively. In addition to the cylindrical objects, there are line objects in the phantom for testing the resolution of imaging systems. The boxes by dashed lines around the cylindrical objects and some of the line objects in Fig. 1 are the areas where the images are to be constructed. The phantom has a frequency-dependent attenuation of about 0.5 dB/MHz/cm.

Two array transducers are used in the experiment (Lu 1998a). One has an aperture of 18.288 mm, 2.25-MHz center frequency, 12.192 mm elevation dimension, element spacing of 0.381 mm and 48 elements. The other has a dimension of 38.4 mm × 10 mm, 2.5-MHz center frequency, 0.6-mm element spacing and 64 elements. Both arrays have no focusing in the elevation direction. For simplicity, no matching circuits were used and, thus, the −6-dB pulse-echo bandwidths of the transducers are smaller than 40% of their center frequencies.

2-D images (cross-sections of the objects in the ATS phantom) were constructed by transmitting a plane wave, eqn (2), with the transducers. Echoes received at the elements were weighted with the limited diffraction array beams [eqn (3), where, for a 1-D array, the spatial frequency, k_y , is zero]. The weighted signals were digitized at 20 mega samples/s at 12-bit resolution, compensated for the attenuation with a time-gain-control (TGC) circuit, Fourier transformed in terms of time, eqn (16), interpolated in the k'_z dimension, and then inversely Fourier transformed in space to construct images.

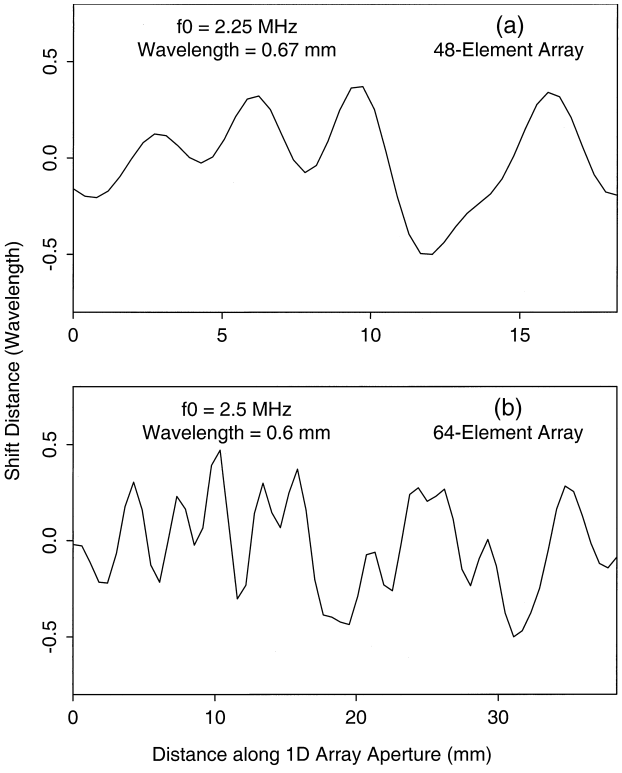

Fig. 2. Random phase shifts of echo signals of linear arrays of (a) 18.288-mm and (b) 38.4-mm apertures.

To introduce phase aberration, echoes received were randomly shifted in time (or distance in terms of wavelength) over the transducer apertures (Fig. 2) before image constructions. The magnitude of the random shift is 0.5 wavelengths (or π in phase) in Fig. 2. Images constructed with no phase shift (magnitude is zero), 0.25 wavelengths (0.5 π in magnitude) and 0.5 wavelengths (π in magnitude) are shown in Figs. 3, 4, and 5, respectively. For comparison, the same sets of experiment data were used to construct images with the conventional delay-and–sum (dynamic focusing) method (Figs. 6, 7 and 8, corresponding to Figs. 3, 4 and 5, respectively). A comparison of these images shows that the phase aberration has a similar effect on both the HFR and the conventional delay-and–sum (dynamic focusing) methods.

To study the effects of the phase aberration quantitatively, contrast of the cystic objects in Figs. 3–-5 was plotted vs. the degree of the phase aberration (Fig. 9a) using the formula

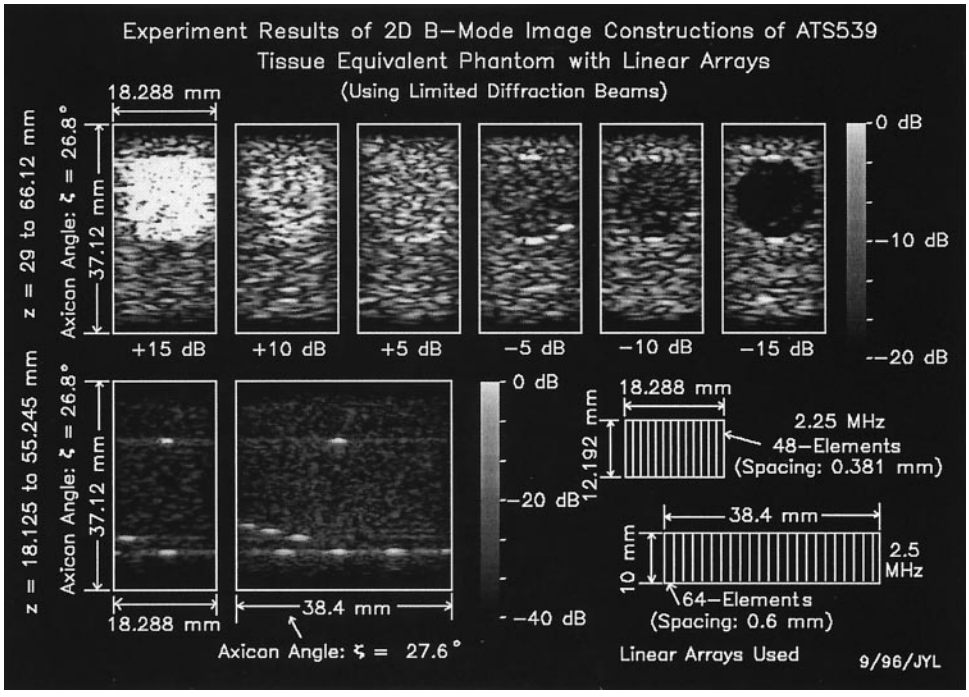

Fig. 3. 2-D B-mode images of the ATS539 tissue-equivalent phantom (Fig. 1) constructed with the HFR method developed from limited diffraction beams without phase aberration. Panels in the top row correspond to constructed images (cross-sections) of the cylindrical grey-scale objects. Panels in the bottom row are images of line objects. The dimensions and the locations of the images in the phantom are shown in both this Fig. and Fig. 1. Dark areas near the top and bottom of each image result from Blackman windows added to A-lines near these regions to reduce potential aliasing in image constructions (reproduced from Fig. 4 of Lu 1998a, with permission).

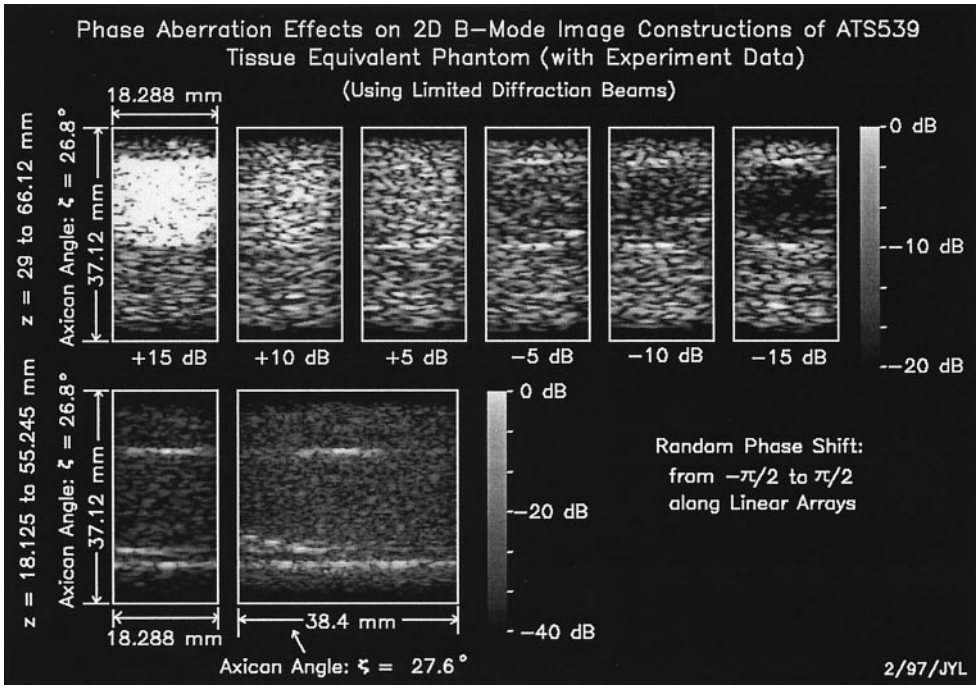

Fig. 4. The same as Fig. 3, except that there is a phase shift from $-\pi/2$ to $\pi/2$ (-0.25 to 0.25 wavelengths) (see the curves in Fig. 2) for echo signals received by the array elements.

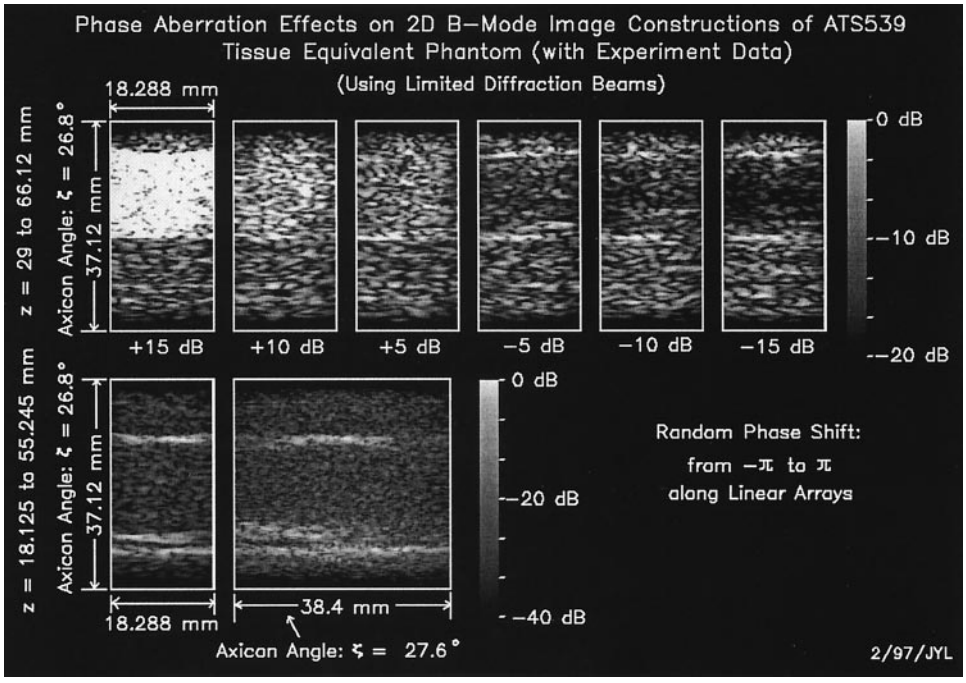

Fig. 5. The same as Fig. 3, except that the phase shift is larger (from $-\pi$ to π, or from -0.5 to 0.5 wavelengths) with the curves in Fig. 2 for echo signals received by the array elements.

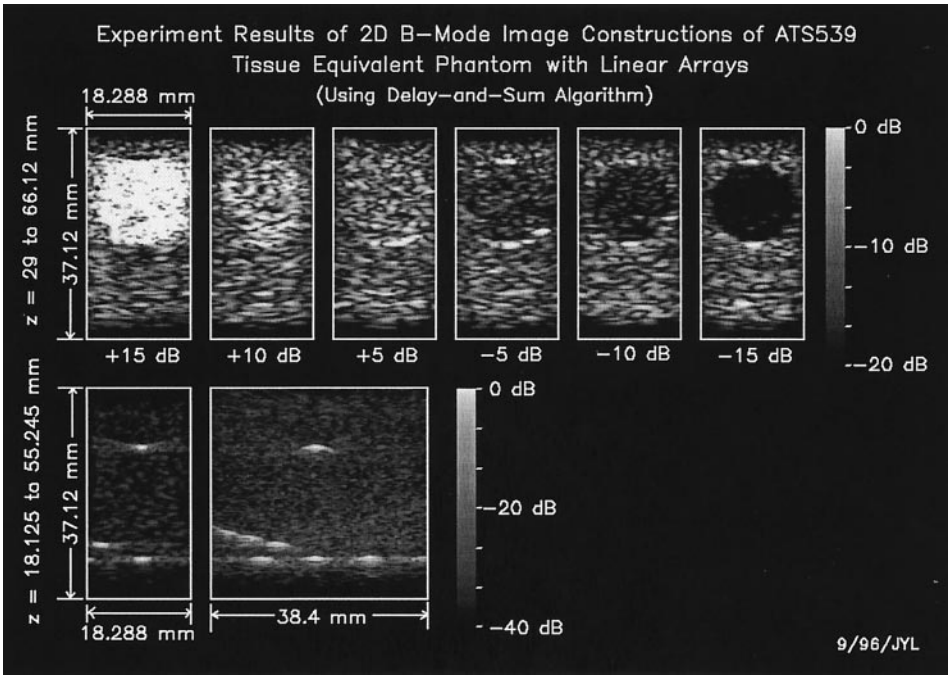

Fig. 6. 2-D B-mode images of the ATS539 tissue-equivalent phantom constructed from the same experimental data as those used in Fig. 3, but with the delay-and–sum algorithm (dynamic focusing at each pixel of RF images). The conditions of the experiment and the format of the Fig. are the same as those of Fig. 3 (reproduced from Fig. 5 of Lu 1998a, with permission).

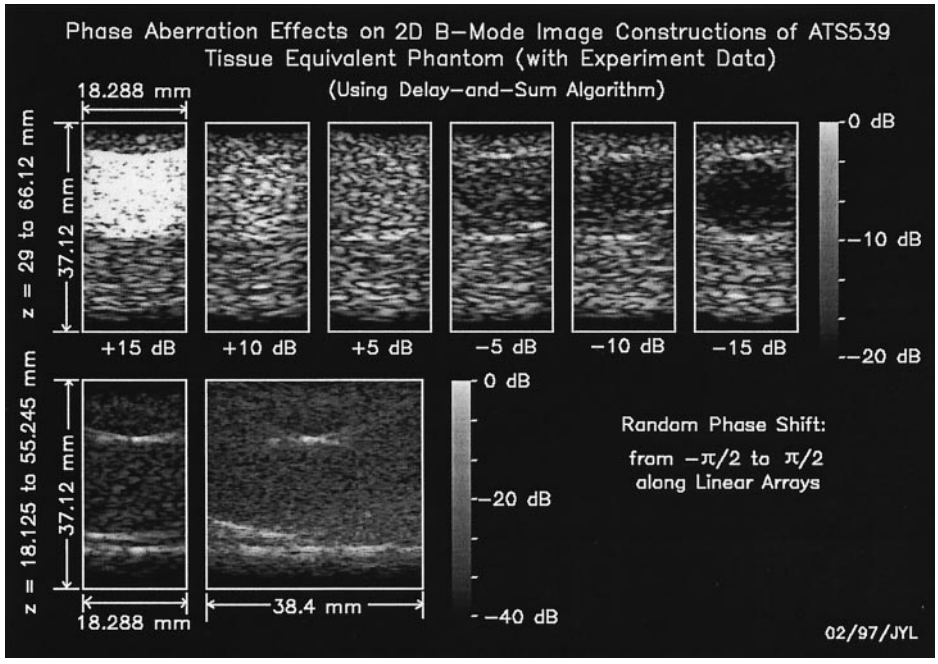

Fig. 7. The same as Fig. 6, except that there is a phase shift from $-\pi/2$ to $\pi/2$ (-0.25 to 0.25 wavelengths) (see the curves in Fig. 2) for echo signals received by the array elements.

$$\text{Contr} = 20 \log_{10} \left| \frac{m_i}{m_o} \right| , \qquad (21)$$

where m_i and m_o are mean reflectivities of the scatterers inside and outside of the cysts. In Fig. 9, the contrast is normalized with respect to its positive and negative maxima. For comparison, the contrast was also plotted for the images (Figs. 6–8) constructed with the delay-and–sum method (Fig. 9b).

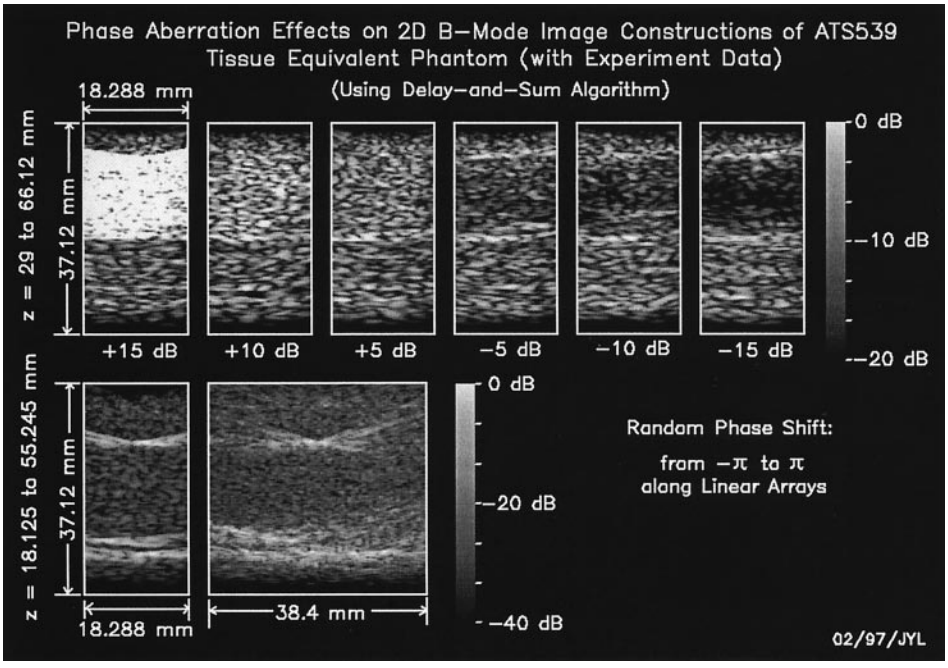

Fig. 8. The same as Fig. 6, except that the phase shift is larger (from $-\pi$ to π, or from -0.5 to 0.5 wavelengths) with the curves in Fig. 2 for echo signals received by the array elements.

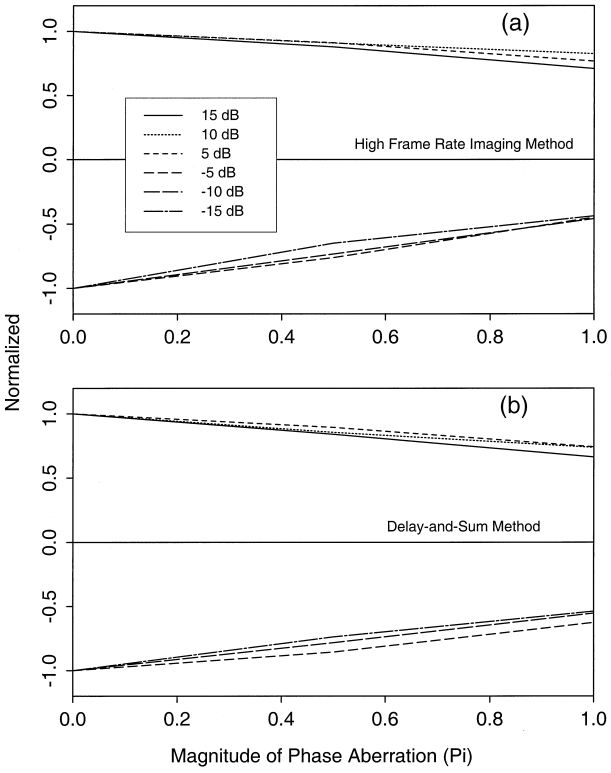

Fig. 9. Normalized contrast, eqn (21), as a function of the magnitude of the phase shift of the echo signals received by the array elements for images of various cylindrical objects (see Fig. 1) constructed with (a) the HFR and (b) delay-and–sum methods.

DISCUSSION

An experiment was performed to construct images of the cross-sections of both the cylindrical and line objects of an ATS 539 tissue-equivalent phantom with and without phase aberration using two different linear-array transducers. Both HFR and the conventional delay-and–sum methods were used in the image constructions. Results show that images constructed with the HFR imaging method are not more sensitive to the phase aberration distortions than those constructed with the conventional method, although imaging systems based on limited diffraction beams could be much simpler. The influence of phase aberration on transmit beams has not been studied in this paper, but is expected to be about the same for both the HFR and the delay-and–sum methods. This can be seen by comparing Figs. 3 and 6, where the corresponding images are almost identical.

When there is phase aberration, resolution and contrast of images constructed with both limited diffraction beams and the delay-and–sum methods decrease (Fig. 9). The greater the phase aberration (random phase shifts), the lower are the resolution and contrast of the images. However, the degradation of the quality of the images is about the same for both methods.

Many methods have been developed to estimate and correct the phase aberration effects (Foster and Hunt 1979; Flax and O'Donnell 1988; O'Donnell and Flax 1988; Trahey et al. 1991; Zhao and Trahey 1991; Zhao et al. 1992; Nock and Trahey 1992; Trahey and Nock 1992; Krishnan et al. 1995, 1996; Li and O'Donnell 1995). For example, the parallel adaptive receive compensation algorithm (PARCA) that uses multiple receive beams to compensate for the imperfect beam forming (Krishnan et al. 1996) is one such method. Using multiple receive beams from different transmit directions, image artefacts due to imperfect beam forming can be identified and greatly reduced. The specific compensation method that uses multiple receive beams and a total least squares (TLS) model of scatterer interaction with acoustic waves to both predict and remove artefacts due to imperfect beam forming (Li and O'Donnell 1995) is yet another technique. Finally, the two-step correction method that is used to improve image quality for large array imaging (Krishnan et al. 1995) could be used. The applicability of all these methods to the HFR imaging method is based on both the simulation and experiment results indicating that the HFR and the conventional delay-and–sum methods are almost identical (see Figs. 3 and 6, and Lu 1998a).

CONCLUSION

Phase-aberration effects are studied for both the newly developed HFR imaging method using limited diffraction beams (Lu 1997a, 1998a) and the conventional delay-and–sum method (Shen et al. 1995). Results indicate that the HFR method is not more sensitive to the phase aberration than the conventional method, although it is robust for image constructions and can be implemented with simpler imaging systems.

Acknowledgments—This work was supported in part by the grant HL60301 from the National Institutes of Health.

REFERENCES

Bailes DR, Bryant DJ. NMR imaging. Contemp Phys 1984;25:441–475.

Bohs LN, Trahey GE. A novel method for angle independent ultrasonic imaging of blood flow and tissue motion. IEEE Trans Biomed Imag 1991;38(3):280–286.

Bohs LN, Friemel BH, McDermott BA, Trahey GE. A real time system for quantifying and displaying two-dimensional velocities using ultrasound. Ultrason Med Biol 1993;19(9):751–761.

Bohs LN, Friemel BH, Trahey GE. Experimental velocity profiles and volumetric flow via two-dimensional speckle tracking. Ultrason Med Biol 1995;21(7):885–898.

Bracewell R. The Fourier transform and its applications. New York: McGraw-Hill; 1965.

Brittingham JN. Focus wave modes in homogeneous Maxwell's equations: transverse electric mode. J Appl Phys 1983;54(3):1179–1189.

Bronskill MJ, Sprawls P. The physics of MRI—1992 AAPM Summer School Proceedings. Woodbury, NY: American Institute of Physics, 1993.

Burckhardt CB, Grandchamp PA, Hoffmann H. Methods for increasing the lateral resolution of B-scan. In: Green PS, ed. Acoustical holography. New York, NY: Plenum Press, 1973a:391–413.

Burckhardt CB, Hoffmann H, Grandchamp PA. Ultrasound axicon: adevice for focusing over a large depth. J Acoust Soc Am 1973b; 54(6):1628–1630.

Donnelly R, Power D, Templeman G, Whalen A. Graphic simulation of superluminal acoustic localized wave pulses. IEEE Trans Ultrason Ferroelec Freq Contr 1994;41(1):7–12.

Durnin J. Exact solutions for nondiffracting beams. I. The scalar theory. J Opt Soc Am 1987;4(4):651–654.

Durnin J, Miceli JJ Jr, Eberly JH. Diffraction-free beams. Phys Rev Lett 1987;58(15):1499–1501.

Flax SW, O'Donnell M. Phase aberration correction using signals from point reflector and diffuse scatterers: Basic principles. IEEE TransUltrason Ferroelec Freq Contr 1988;35(6):758–767.

Foster FS, Hunt JW. The focusing of ultrasound beams throughhuman tissue. In: Metherell AF, ed. Acoustical imaging. Vol. 8. New York: Plenum Press; 1979:709–718.

Foster FS, Larson JD, Mason MK, Shoup TS, Nelson G, Yoshida H. Development of a 12 element annular array transducer for realtime ultrasound imaging. Ultrasound Med Biol 1989;15(7):649–659.

Krishnan S, Li P-C, O'Donnell M. Two-step aberration correction.Ultrason Imaging Tissue Characterization 1995;17:62–63.

Krishnan S, Li P-C, O'Donnell M. Adaptive compensation of phase and magnitude aberrations. IEEE Trans Ultrason Ferroelec Freq Contr 1996;43(1):44–55.

Li P-C, O'Donnell M. Phase aberration correction on two-dimensionalconformal arrays. IEEE Trans Ultrason Ferroelec Freq Contr 1995;42(1):73–82.

Lu J-Y. Improving accuracy of transverse velocity measurement with anew limited diffraction beam. IEEE Ultrason Symp Proc 1996;2: 1255–1260.

Lu J-Y. 2-D and 3-D high frame rate imaging with limited diffractionbeams. IEEE Trans Ultrason Ferroelec Freq Contr 1997a;44(4): 839–856.

Lu J-Y. Transmit-receive dynamic focusing with limited diffractionbeams. IEEE Ultrason Symp Proc 1997b;2:1543–1546.

Lu J-Y. Designing limited diffraction beams. IEEE Trans Ultrason Ferroelec Freq Contr 1997c;44(1):181–193.

Lu J-Y. Limited diffraction array beams. Int J Imaging Syst Technol 1997d;8(1):126–136.

Lu J-Y. Experimental study of high frame rate imaging with limited diffraction beams. IEEE Trans Ultrason Ferroelec Freq Contr 1998a;45(1):84–97.

Lu J-Y. A study of signal-to-noise ratio of the Fourier method for construction of high frame rate images. Acoust Imaging 1998b (In press).

Lu J-Y, Greenleaf JF. Ultrasonic nondiffracting transducer formedical imaging. IEEE Trans Ultrason Ferroelec Freq Contr 1990a;37(5): 438–447.

Lu J-Y, Greenleaf JF. Evaluation of a nondiffracting transducerfor tissue characterization. IEEE 1990 Ultrason Symp Proc 1990b;2: 795–798.

Lu J-Y, Greenleaf JF. Theory and acoustic experiments of nondiffracting X waves. IEEE 1991 Ultrason Symp Proc 1991;2:1155–1159.

Lu J-Y, Greenleaf JF. Nondiffracting X waves—exact solutions to free-space scalar wave equation and their finite aperture realizations. IEEE Trans Ultrason Ferroelec Freq Contr 1992a;39(1):19–31.

Lu J-Y, Greenleaf JF. Experimental verification of nondiffracting X waves. IEEE Trans Ultrason Ferroelec Freq Contr 1992b;39(3): 441–446.

Lu J-Y, Greenleaf JF. Producing deep depth of field anddepth-independent resolution in NDE with limited diffraction beams.Ultrason Imag 1993;15(2):134–149.

Lu J-Y, He S. Optical X waves communications. Optic Comm 1999; 161:187–192.

Lu J-Y, Xu X-L, Zou H, Greenleaf JF. Application of Bessel beam for Doppler velocity estimation. IEEE Trans Ultrason Ferroelec Freq Contr 1995;42(4):649–662.

Lu J-Y, Zou H, Greenleaf JF. Biomedical ultrasound beam forming.Ultrasound Med Biol 1994;20(5):403–428.

Nock LF, Trahey GE. Synthetic receive aperture imaging with phase correction for motion and for tissue inhomogeneities—Part I: Basic principles. IEEE Trans Ultrason Ferroelec Freq Contr 1992;39(4): 489–495.

O'Donnell M, Flax SW. Phase aberration correction using signals from point reflector and diffuse scatterers: measurements. IEEE Trans Ultrason Ferroelec Freq Contr 1998;35(6):768–774.

Ojeda-Castaneda J, Noyola-lglesias A. Nondiffracting wavefields in grin and free-space. Microwave Optic Tech Lett 1990;3(12):430–433.

Oppenheim AV, Schafer RW. Digital signal processing. Englewood Cliffs, NJ: Prentice-Hall, 1975.

Ramamurthy BS, Trahey GE. Potential and limitations of angle-independent flow detection algorithms using radio-frequency and detected echo signals. Ultrason Imag 1991;13:252–268.

Shattuck DP, Weinshenker MD, Smith SW, von Ramm OT. Explososcan: A parallel processing technique for high speed ultrasound imaging with linear phased arrays. J Acoust Soc Am 1984; 75(4):1273–1282.

Shen J, Wang H, Cain C, Ebbini ES. A post-beam forming processing technique for enhancing conventional pulse-echo ultrasound imaging contrast resolution. EEE Ultrason Symp Proc 1995;2:1319–1322.

Silverstein SD, O'Donnell M. Frequency and temporal compounding of partially correlated signals: speckle suppression and image resolution.SPIE Visual Communic Image Processing II 1987;845:188–194.

Song TK, Lu J-Y, Greenleaf JF. Modified X waves with improved field properties. Ultrason Imag 1993;15(1):36–47.

Stratton JA. Electromagnetic theory. New York, London: McGraw-Hill, 1941:356.

Trahey GE, Nock LF. Synthetic receive aperture imaging with phase correction for motion and for tissue inhomogeneities—Part II: Effects of and correction for motion. IEEE Trans Ultrason Ferroelec Freq Contr 1992;39(4):489–495.

Trahey GE, Freiburger PD, Nock LF, Sullivan DC. In vivo measurements of ultrasonic beam distortion in the breast. Ultrason Imag 1991;13:71–90.

Trahey GE, Hubbard SM, von Ramm OT. Angle independent ultrasonic blood flow detection by frame-to-frame correlation of B-mode images. Ultrasonics 1988;26:271–276.

Trahey GE, Smith SW, von Ramm OT. Speckle reduction in medical ultrasound via spatial compounding. SPIE Med XIV PACS, 1986; 4:626–637.

Wells PNT. Biomedical ultrasonics. New York: Academic Press, 1977.

Zhao D, Trahey GE. Comparisons of image quality factors for phase aberration correction with diffuse and point targets: Theory and experiments. IEEE Trans Ultrason Ferroelec Freq Contr 1991; 38(2):125–132.

Zhao D, Bohs LN, Trahey GE. Phase aberration correction using echo signals from moving targets I: Description and theory. Ultrason Imag 1992;14:97–110.

Ziolkowski RW. Exact solutions of the wave equation with complex source locations. J Math Phys 1985;26(4):861–863.

Ziolkowski RW, Lewis DK, Cook BD. Evidence of localized wave transmission. Phys Rev Lett 1989;62(2):147–150.